EUV Experimental Physics of Extreme Ultraviolet

RWTH AACHEN UNIVERSITY

JÜLICH FORSCHUNGSZENTRUM

Application of lens-less imaging techniques for nano-scale microscopy employing plasma-based EUV source

Larissa Juschkin
RWTH Aachen University

Jan Bußmann, Raoul Bresenitz, Denis Rudolf
Peter Grünberg Institut 9, Forschungszentrum Jülich

Michal Odstrcil
University of Southampton

RWTH-EUV

EUV Experimental Physics of Extreme Ultraviolet | RWTH AACHEN UNIVERSITY

JÜLICH FORSCHUNGSZENTRUM

Chair for Experimental Physics of Extreme Ultraviolet
Physics Department of the Faculty of Natural Science, Informatics and Mathematics
RWTH Aachen University

- started in 2012
- based at Fraunhofer Institute for Laser Technology, Steinbachstr. 15, 52074 Aachen, Germany
- collaborating with Chair for Technology of Optical Systems (TOS), RWTH Aachen

&

EUV Lithography and Spectroscopy group
at Peter Grünberg Institute 9
Semiconductor Nanoelectronics
in Forschungszentrum Jülich

- started in 2013

JARA | FIT Fundamentals of Future Information Technology

HELMHOLTZ GEMEINSCHAFT

Fraunhofer ILT

TOS Chair for Technology of Optical Systems | RWTH AACHEN UNIVERSITY

EXTATIC

Erasmus Mundus

Our fields of research

- Applications of extreme ultraviolet radiation in nanostructuring and metrology including
  - ✓ EUV microscopy and imaging
  - ✓ EUV lithography and nanostructuring
  - ✓ Scatterometry and coherent diffractive imaging
  - ✓ Soft X-ray and EUV spectroscopy and reflectometry
  - ✓ Photo-electron emission spectroscopy and microscopy
- Soft X-ray and EUV compact radiation sources

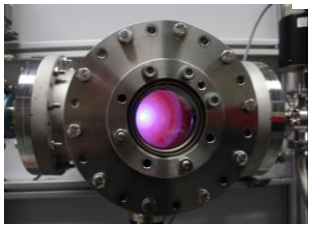

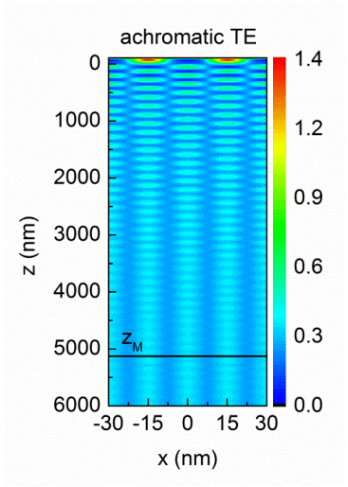

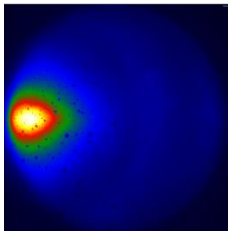

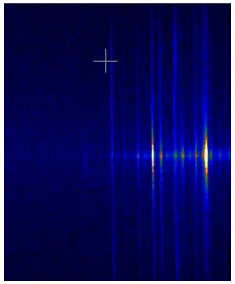

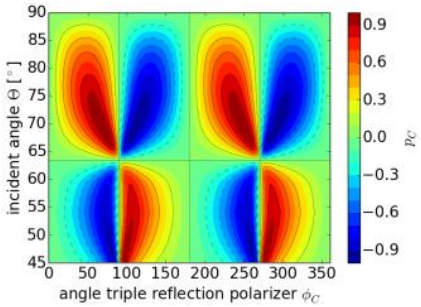

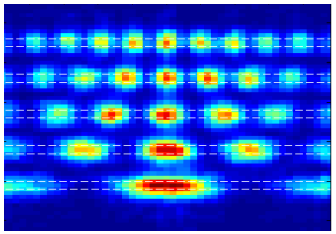

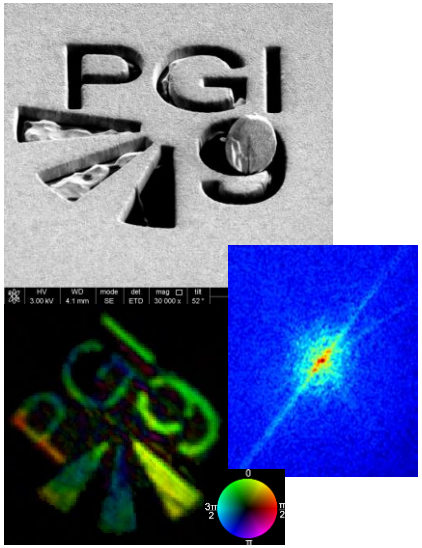

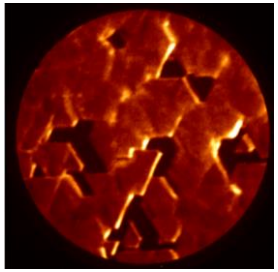

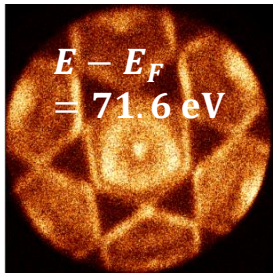

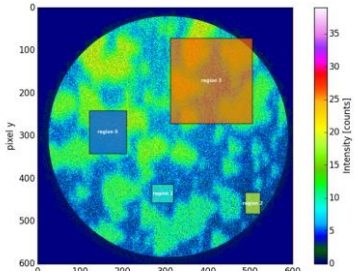

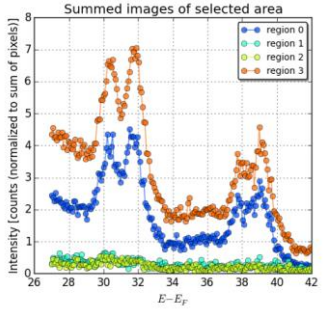

JARA|FIT
Fundamentals of Future Information Technology

Our fields of research

- Applications of extreme ultraviolet radiation in nanostructuring and metrology including
  - ✓ EUV microscopy and imaging
  - ✓ EUV lithography and nanostructuring
  - ✓ **Scatterometry and coherent diffractive imaging**
  - ✓ Soft X-ray and EUV spectroscopy and reflectometry
  - ✓ Photo-electron emission spectroscopy and microscopy
- Soft X-ray and EUV compact radiation sources

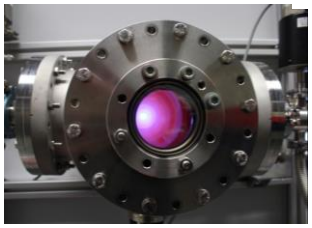

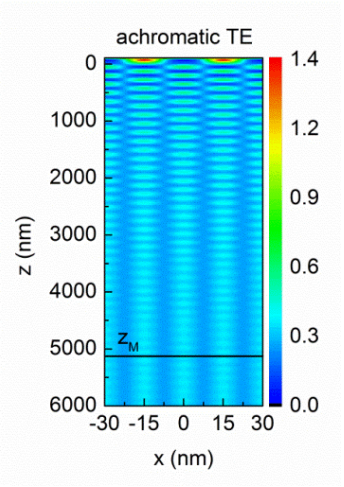

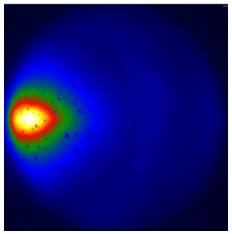

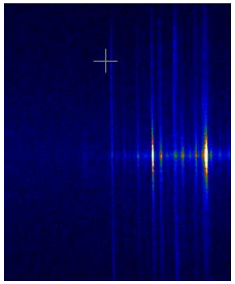

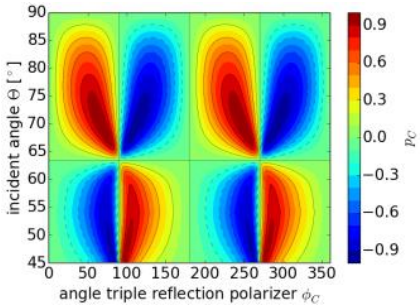

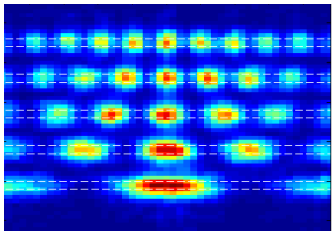

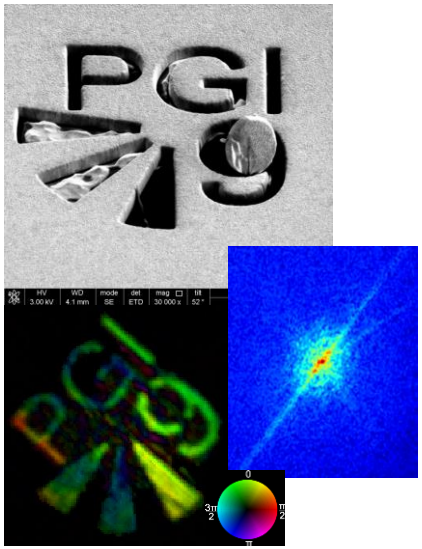

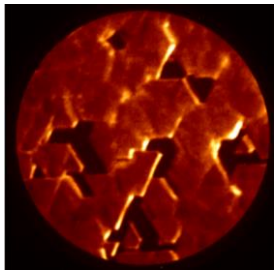

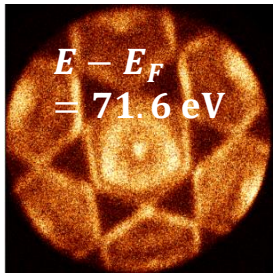

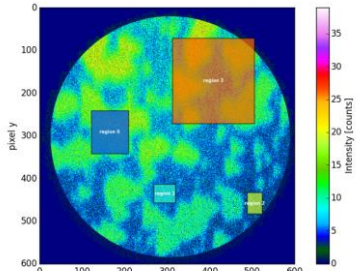

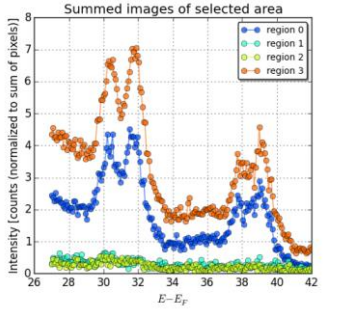

JARA|FIT
Fundamentals of Future Information Technology

Motivation – Why CDI is interesting for us?

CDI advantages comparing to standard optical microscopy:

- Not limited by quality of optics
- Large depth of focus
- More compact setup, easier alignment
- Better use of incidence light => lower dose
- Reconstruction of phase shift and attenuation

particularly suited for imaging with short wavelength radiation

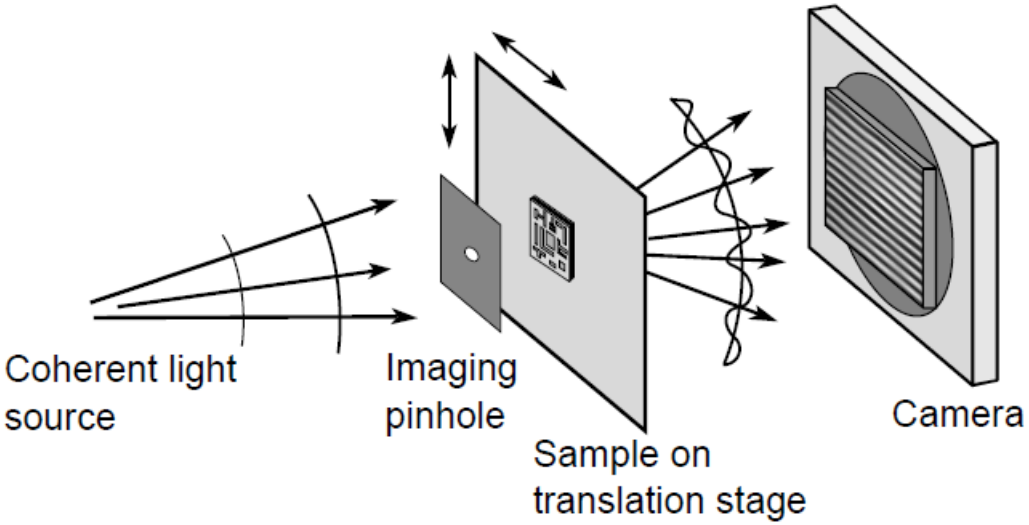

XUV: short wavelength and strong light matter interaction

lateral & in-depth (3d) nm resolutions with element sensitivity and high throughput

Compact 2 kHz source developed at Fraunhofer Institute for Laser Technology

JÜLICH FORSCHUNGSZENTRUM

Plasma-based gas discharge EUV source

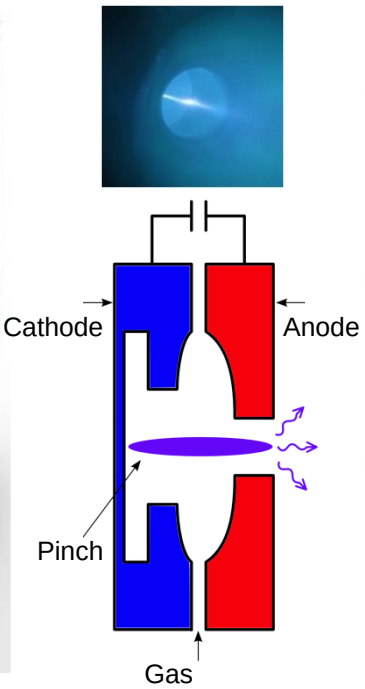

- **input power up to 5.6 kW, 2 kHz**
- **pinch radius down to 100 µm**
- **100W/(mm²sr) radiance @ 10.9 nm**

Emission spectra of nitrogen and oxygen plasmas

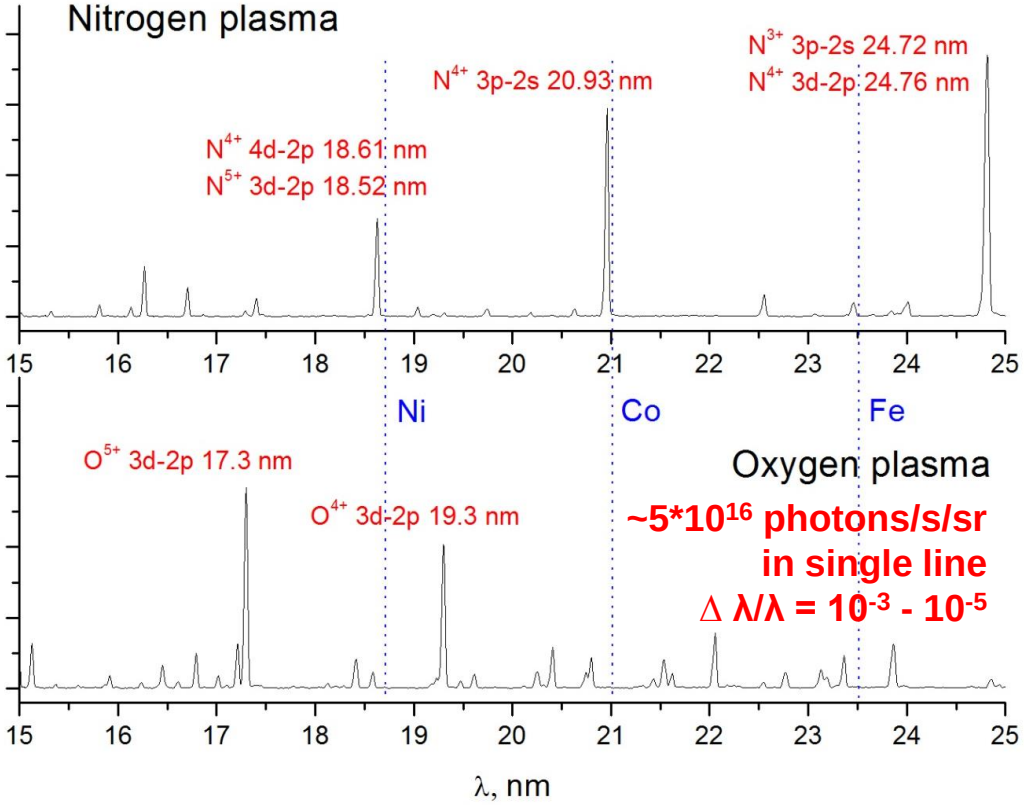

Already successfully used for imaging at 2.88 nm, 13.5 nm and 17.3 nm

Fraunhofer ILT

EUV Experimental Physics of Extreme Ultraviolet | RWTH AACHEN UNIVERSITY

Physical limitations

Limited lateral coherence length

- CDI assumes planar wavefront / unlimited coherence length

Limited temporal coherence length

- Plasma may emit multiple spectral lines

Detector

- Size of the CCD-chip limits maximal resolution
- Pixel size limits the field of view

Source

- Source radiance and exposure time limit achievable resolution

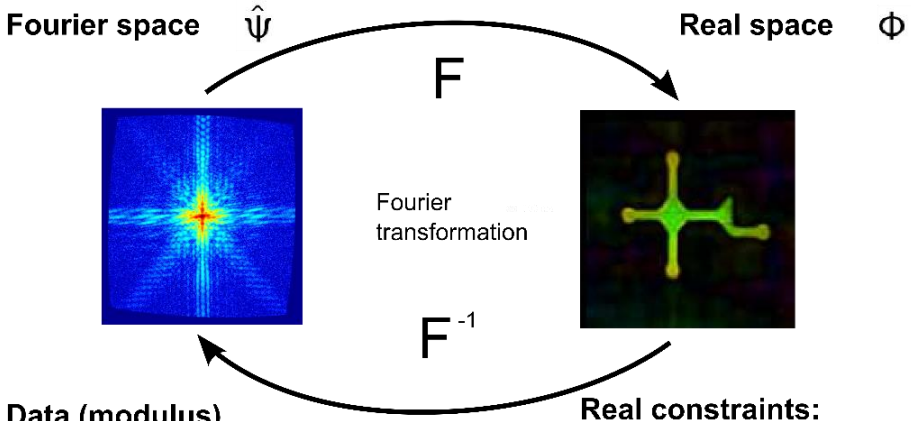

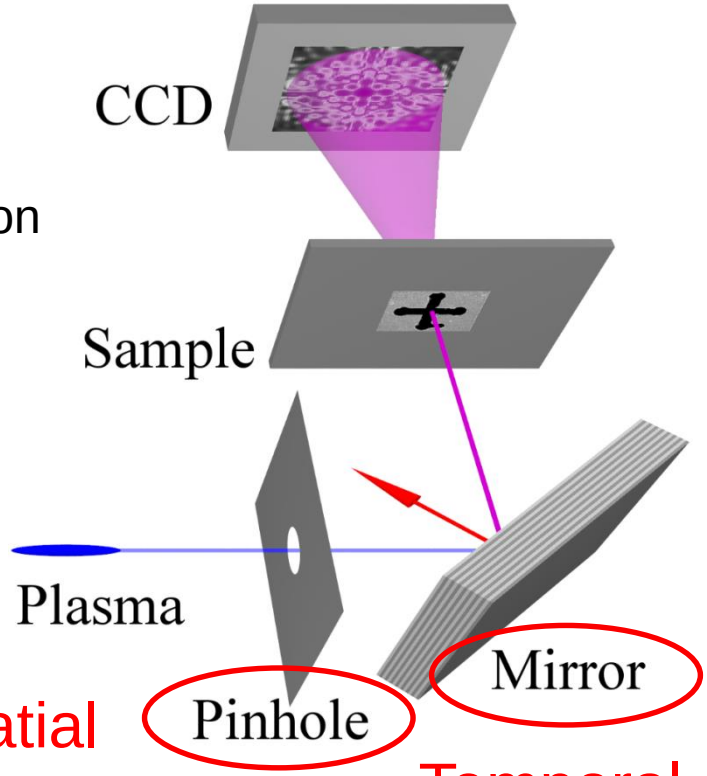

Constraints - temporal coherence

- Polychromatic source leads to distortion at the edges of the diffraction pattern
- Region of high resolution information

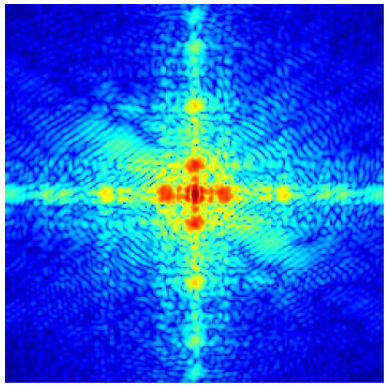

Spectral lines

- Mutliple emission lines over a broad spectral range
- Single emission line is sharp: $\frac{\lambda}{\Delta\lambda} \approx 10^{-4}$
- Imaging wavelength adjustable by working gas and source parameters
- Isolated lines are selectable even by single broad band multilayer EUV filter ($\Delta\lambda = 1\,nm$) and a visible light filter
- ML-Mirror: $[Si/B_4C]_{x50}$, d=13.4 nm, R=0.4, AoI: 46.2°

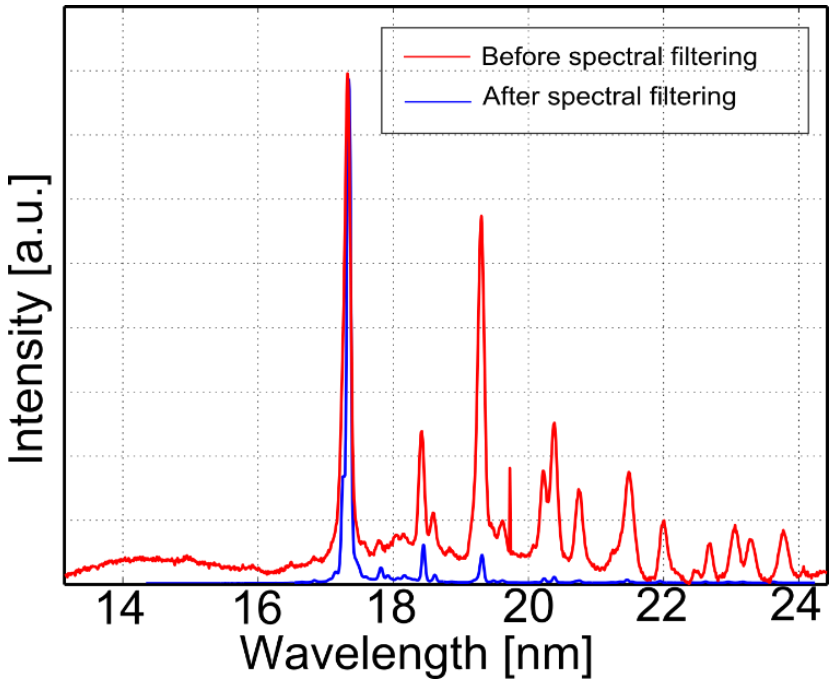

Constraints – spatial coherence

- limits the total size of the sample
- depends strongly on the shape of the source.
- 500 µm pinhole changes the shape to a top-hat Lorentz function
- spatial coherence can be measured by visibility of double slit fringes
- $l_{spatial}$ ~ 14 µm > (object + oversampling) size

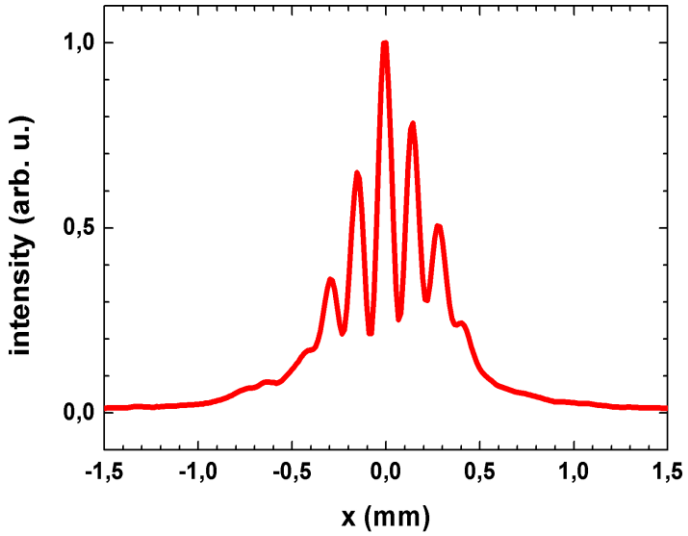

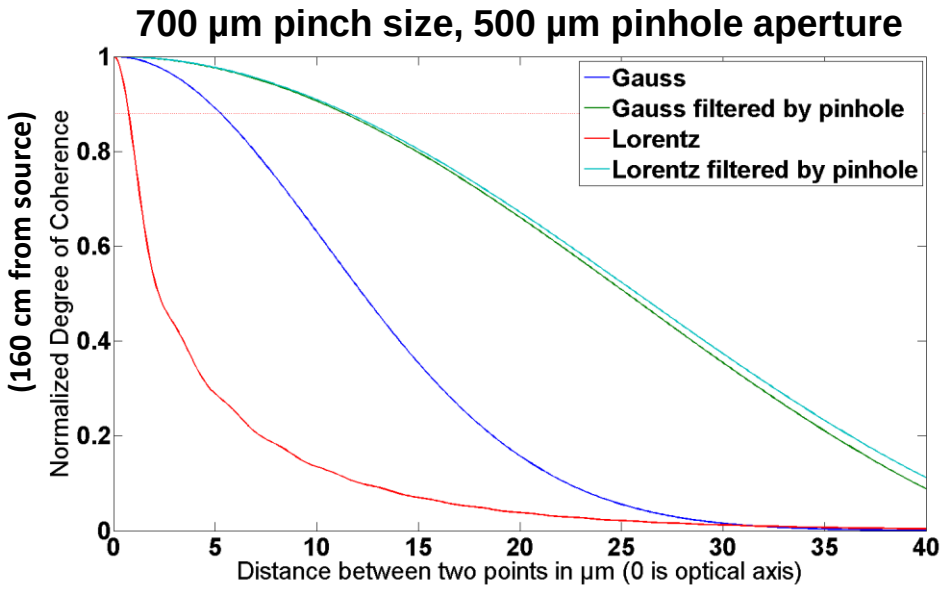

Experimental setup

- Oxygen plasma, 17.3 nm
  O VI 3d - 2p emission line
  40 µJ/sr per pulse
- 0.7-1.5 kHz repetition rate,
  2.3 J discharge energy
- Andor iKon CCD
  1024 x 1024 pixels, 13 µm
- Mirror on a 2-axis tiltable stage
- Sample on a x-y stage

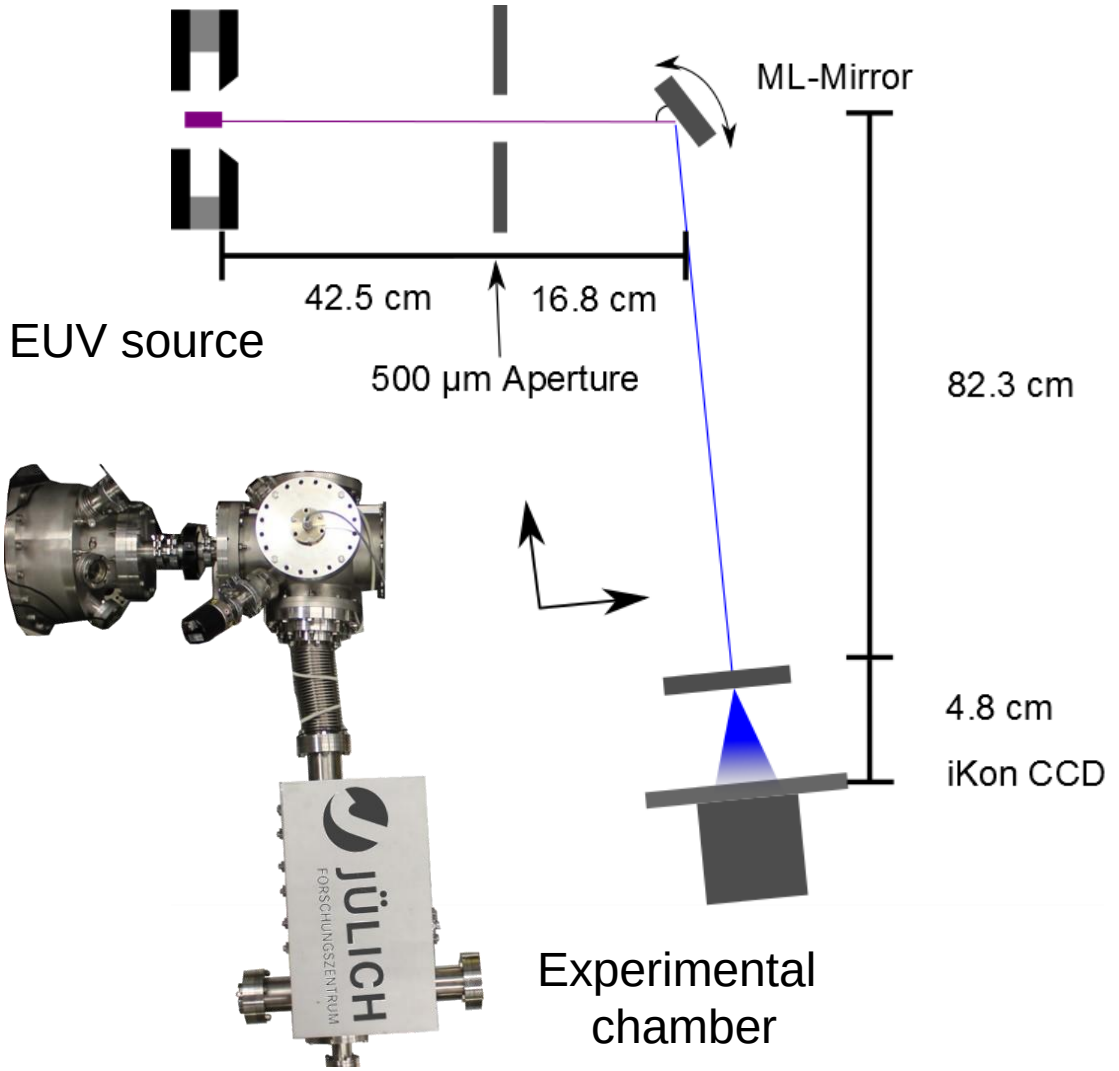

Reconstruction

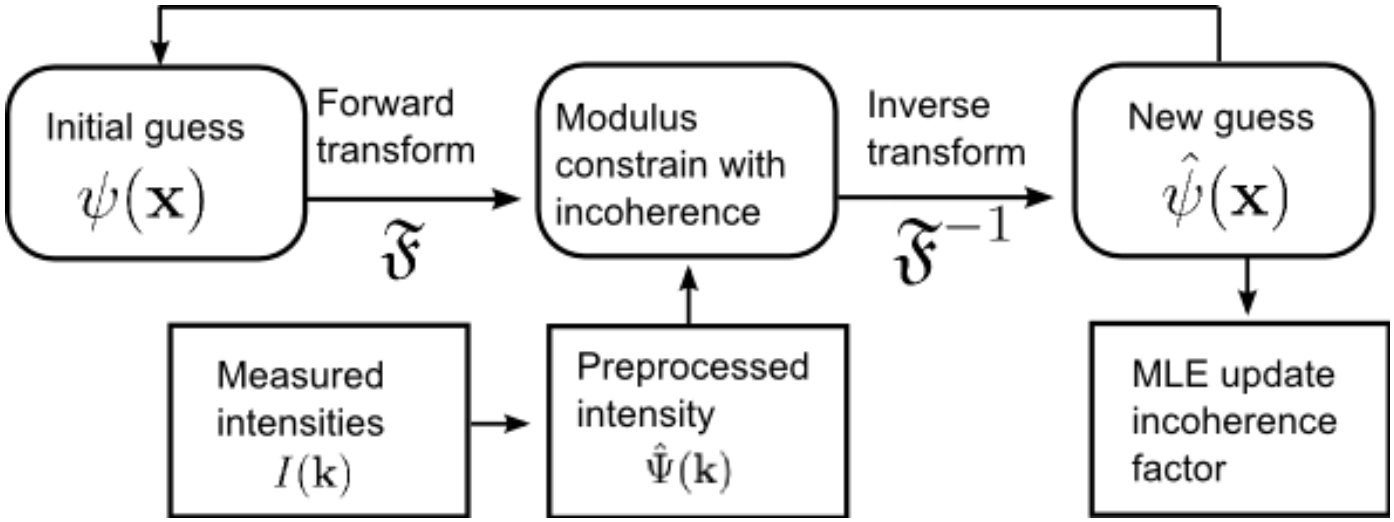

- Deconvolve image to account for partial coherence
- Addition of background diffraction pattern of long wavelengths

$$\left|\Psi_j(\mathbf{k})'\right|^2 = \left|\Psi_j(\mathbf{k})\right|^2 * PSF + b_j$$

Measurement *Ideal diffraction pattern*

Partial coherence

- Partial coherence leads to blurring of diffraction pattern
- Blurring is convolution of the diffraction pattern with point spread function (PSF)
- If deblurring is „stable“ deconvolution is possible

$$\left|\Psi_j(k)'\right|^2 = \left|\Psi_j(k)\right|^2 * PSF$$

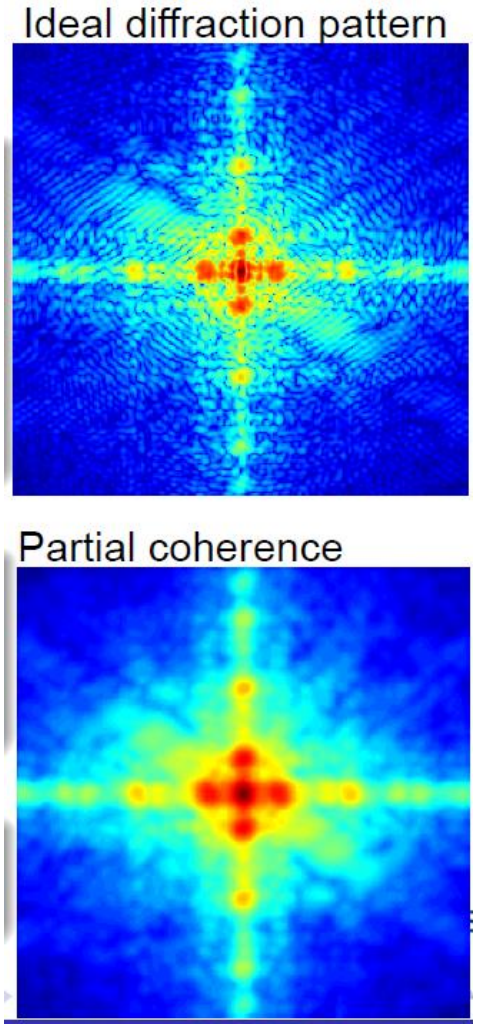

Background light diffraction handling

- Longer wavelengths generate overlapping diffraction patterns
- Filtering removes the UV/Visible light but with loss of overall intensity
- (Realistic) assumption:
  - Low intensity
  - Coherent

⇒ Upscaling of the reconstructed diffraction pattern

$$\left|\Psi_j(k)'\right|^2 = \left|\Psi_j(k)\right|^2 * PSF + b_j$$

⇒ Iterative optimization of the background estimate

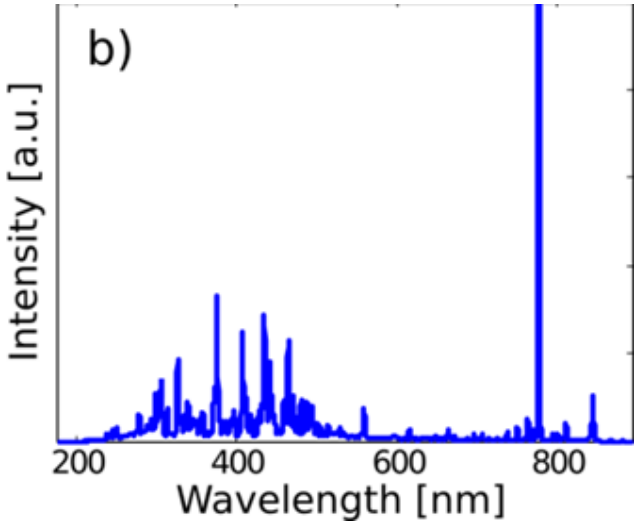

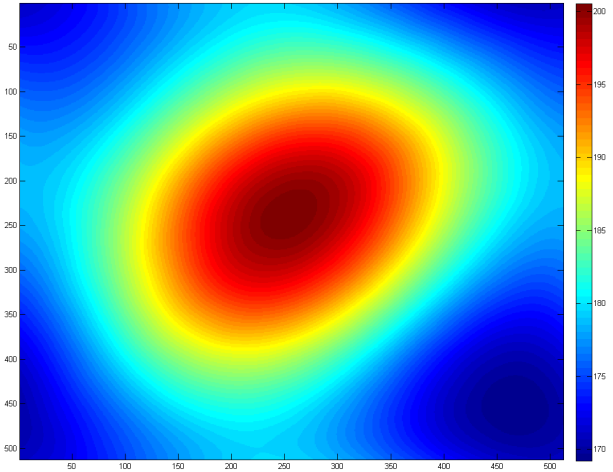

Reconstruction – 1. Cross sample

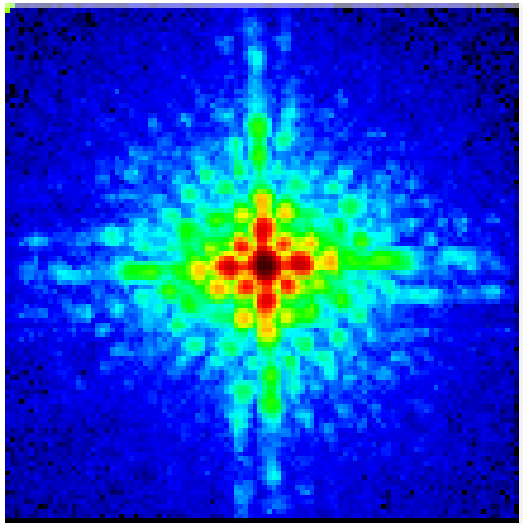

Recorded pattern

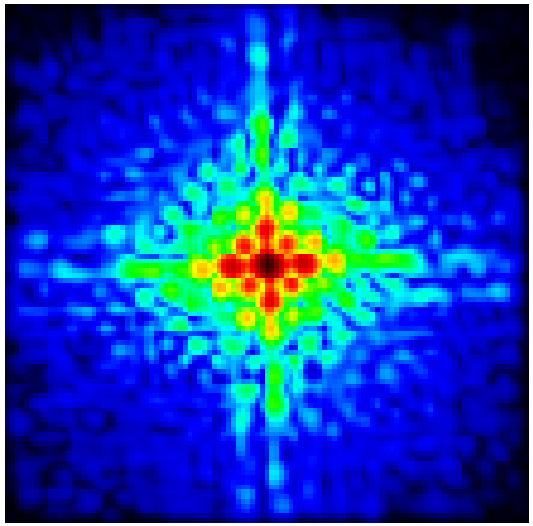

Reconstructed pattern

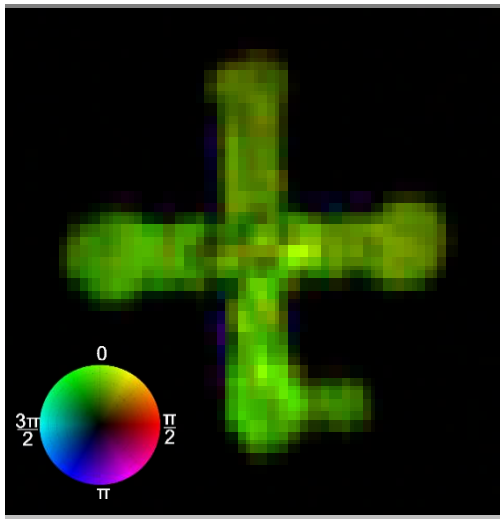

Reconstruction

- 256 px x 256 px (limited by flux)
- 600 s with ~ 10^7 Photons in image
- 200 nm estimated (by PRTF and Knife-Edge)
- Reconstruction of amplitude object

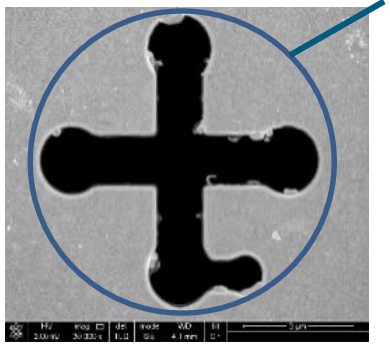

8 µm

400 nm Gold on
200 nm Si_3N_4

Bußmann et al , in X-Ray Lasers 2014, Springer Proc. Phys. ***169****, 275-280 (2016)*

Measurement of phase object

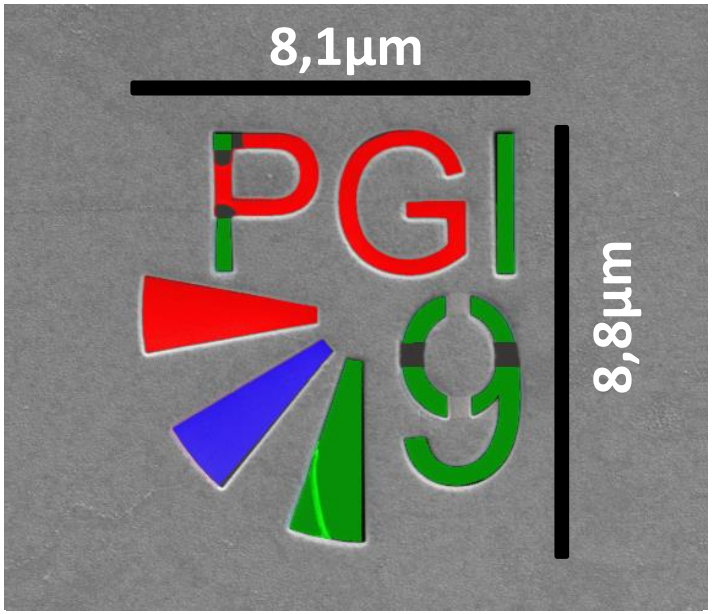

SEM image of sample

=>

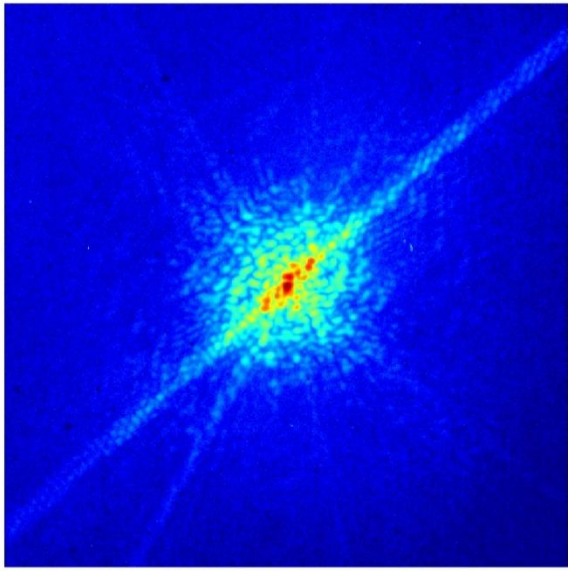

Recorded diffraction pattern

- 500 nm Gold on 200 nm Si_3N_4
- 3 FIB cut areas:
  - completely milled down (green)
  - ~ 50 nm residual Si_3N_4 (red)
  - ~ 200 nm residual Si_3N_4 (blue)

- 512 px x 512 px
- 1000 s integration time

Reconstruction – 2. PGI-Phase

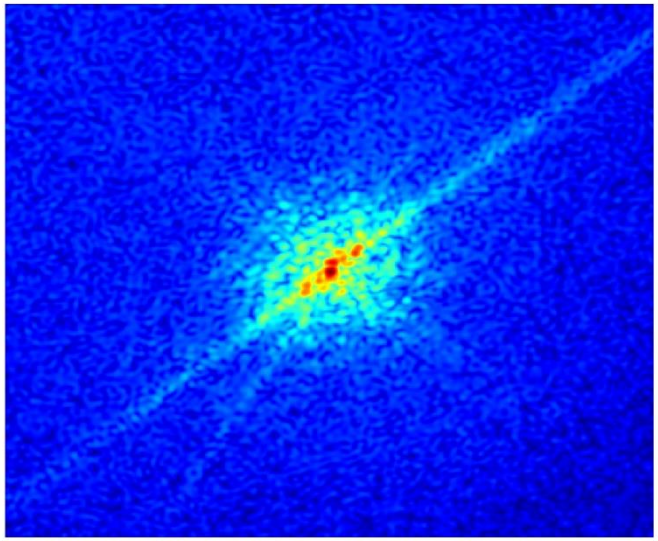

Reconstructed diffraction pattern

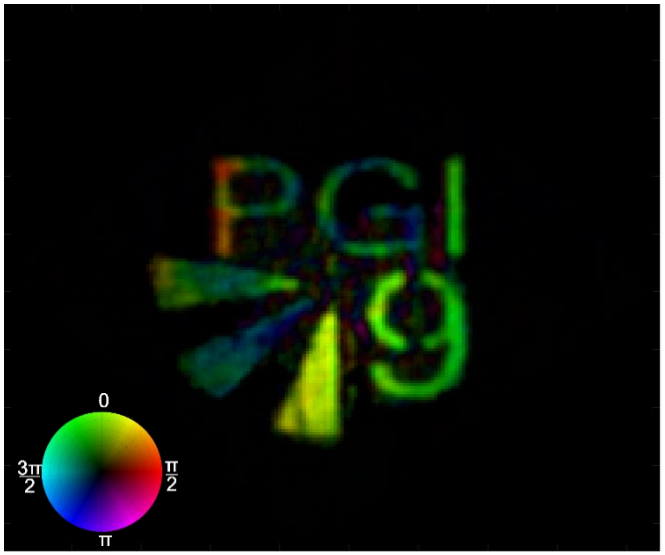

Reconstructed object

- ~ 110 nm resolution
- Visible light background subtraction
- Reconstruction of complex object

=> CDI with pinch plasma gas-discharge sources

J. Bußmann et al., SPIE Proc. ***9589*** *(2015)*

Ptychography

- Scanning Coherent Diffractive Imaging
- Uses overlapping information as real space constrain
  - Nyquist theorem requires an overlap of larger than 50% (in theory)
- Spatial incoherence does not influence field of view but scanning time
- Ptychography needs stable source during measurement
- Multi-wavelength reconstruction: $\Psi_{tot} = \sum a_i |\Psi_i|$

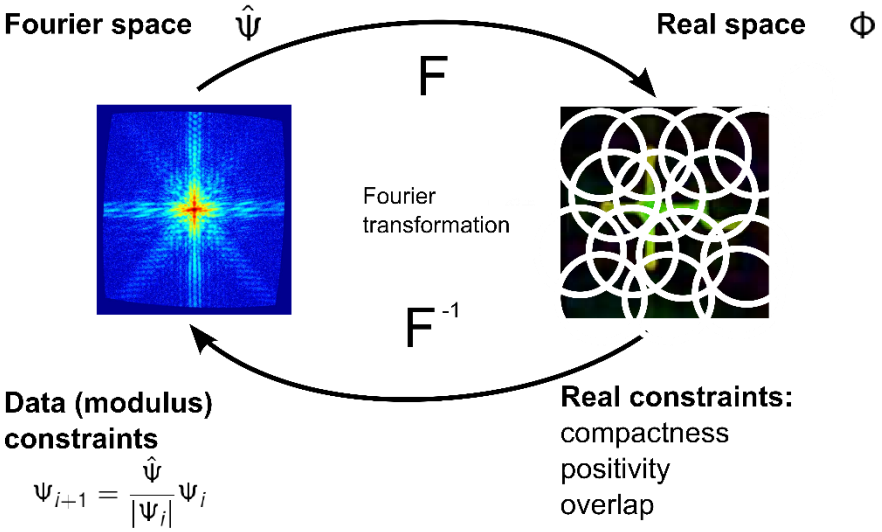

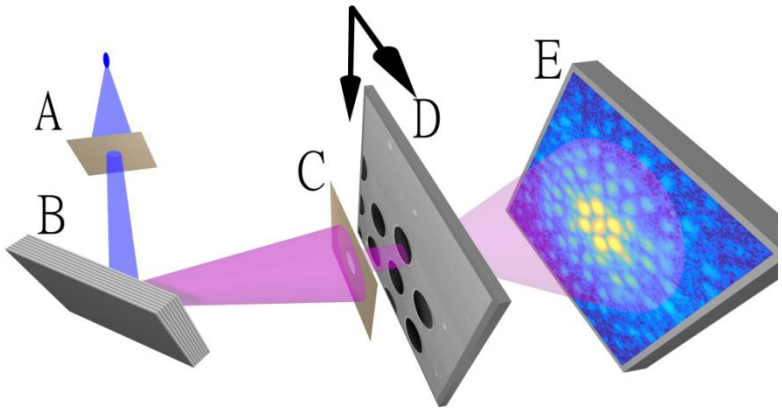

J. M. Rodenburg, H. M. Faulkner, “A phase retrieval algorithm for shifting illumination”, *Applied Physics Letters* **85** (20), 4795 (2004)

Ptychography

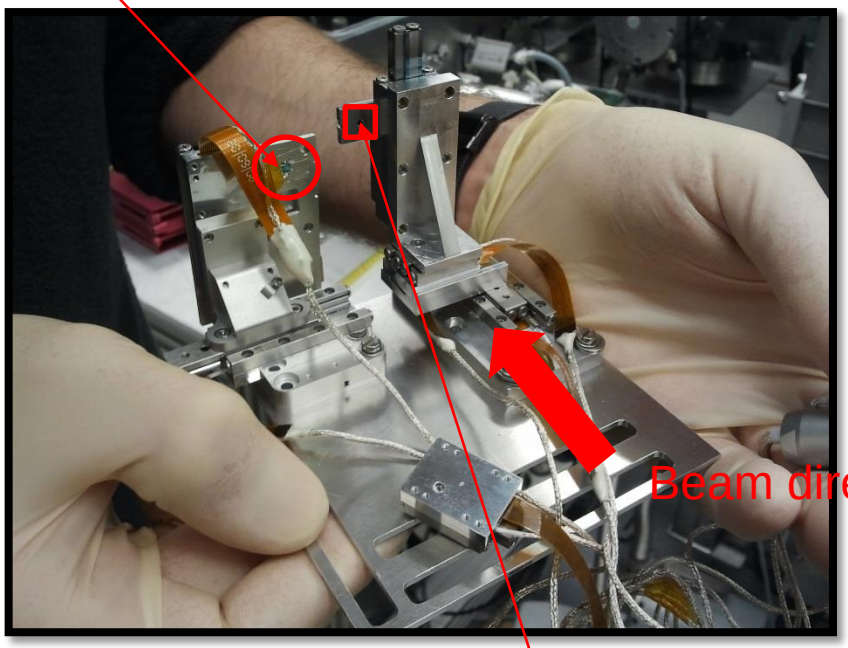

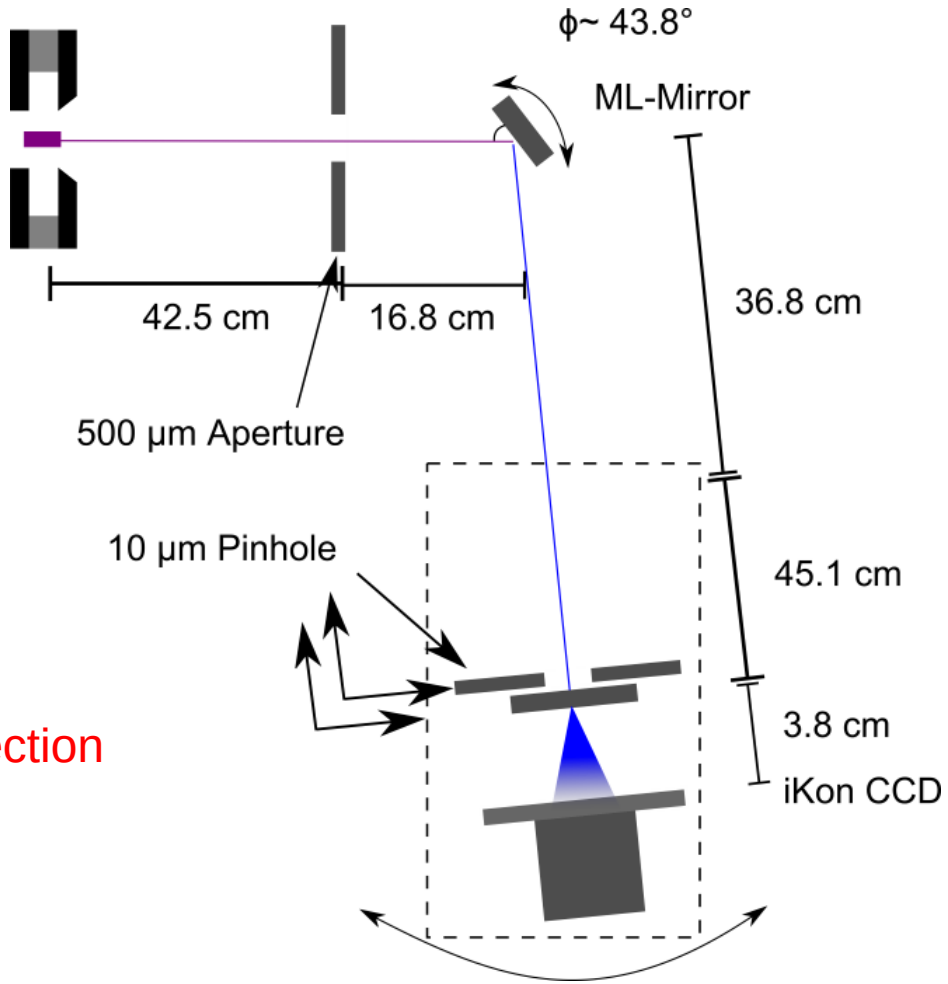

Ptychography on a TEM grid

Sample

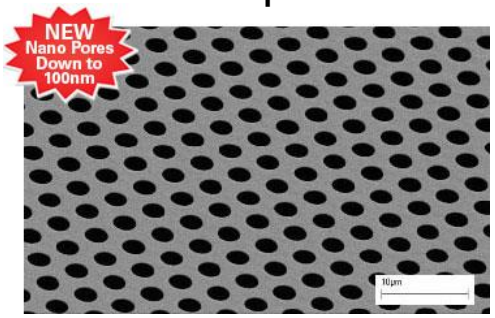

- 200 nm Si_3N_4 membrane
- 2.5 µm holes

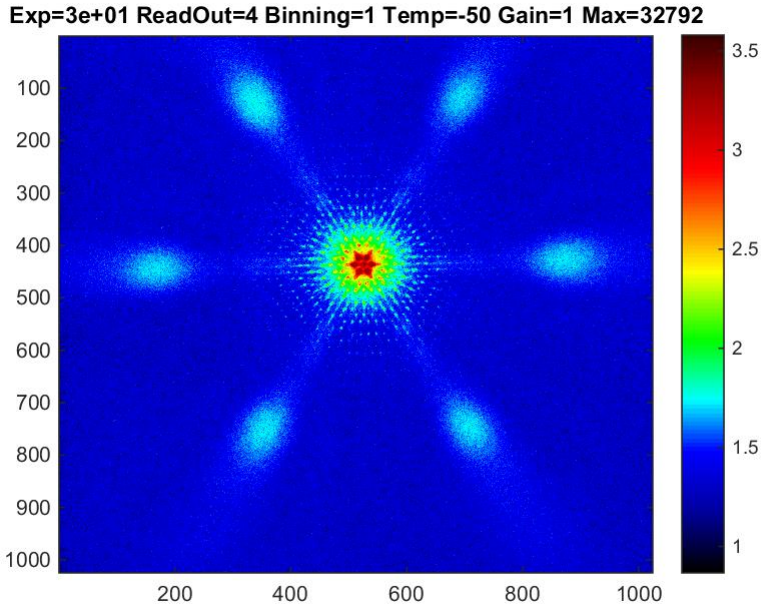

Pinhole

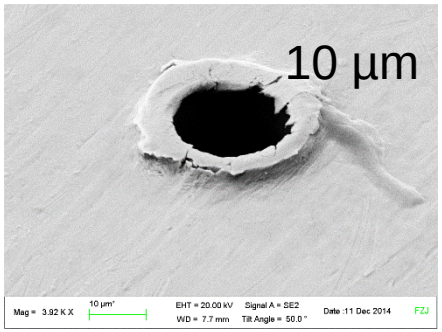

Size limited by spatial coherence

700 µm pinch size, 500 µm aperture

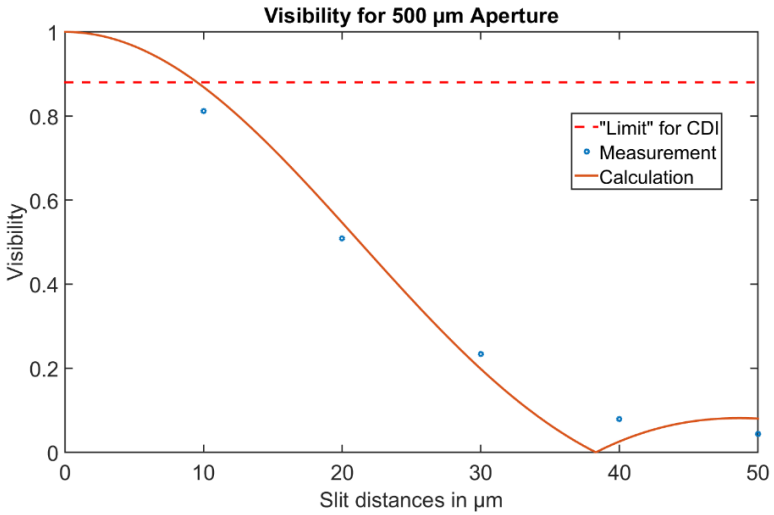

Reconstruction

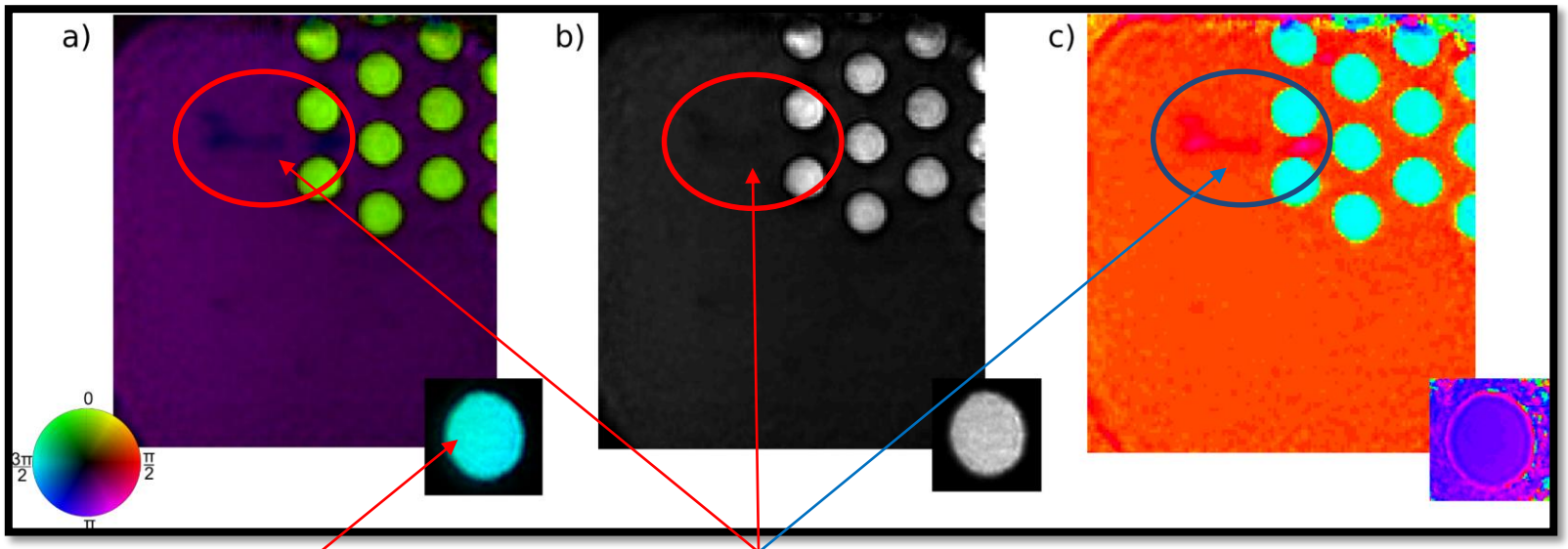

Reconstruction of probe beam

Residual particle visible in phase but only hardly in amplitude

- Lateral resolution: 250 nm @ 30 s per scanning position
- Reconstructed CCD – Sample distance: 44 mm
- Reconstructed membrane thickness: 175 ± 5 nm (SEM: 180 nm, specs: 200 ± 10 nm)

M. Odstrcil, Opt. Lett., (2015), in print

Additionally gained information

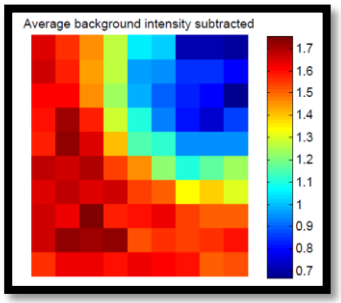

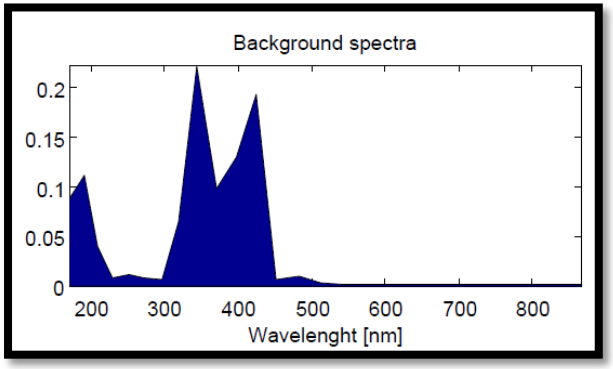

Background subtraction difficult for chromatic materials

18.5 nm Reconstruction

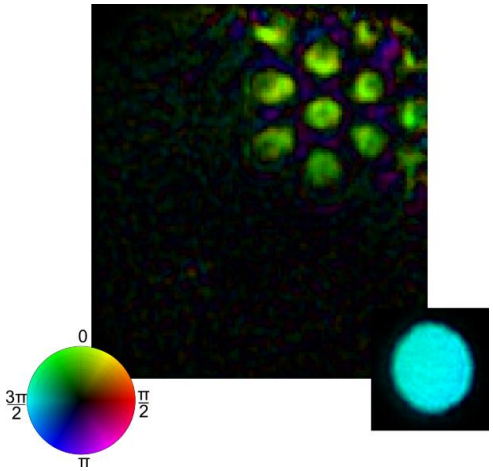

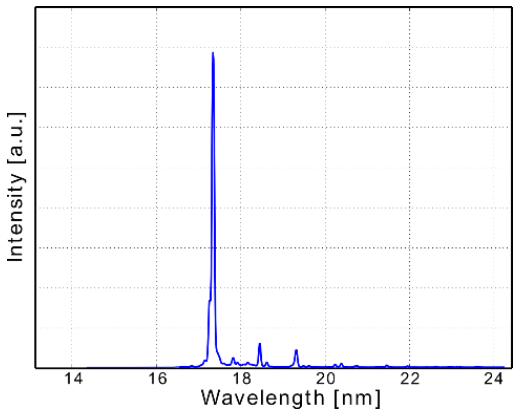

- Shape of object leads to different backgrounds in detector plane
- Chromatic objects (i.e. SiN) require multi-wavelength reconstruction

Reconstruction grid + 200 nm Al foil

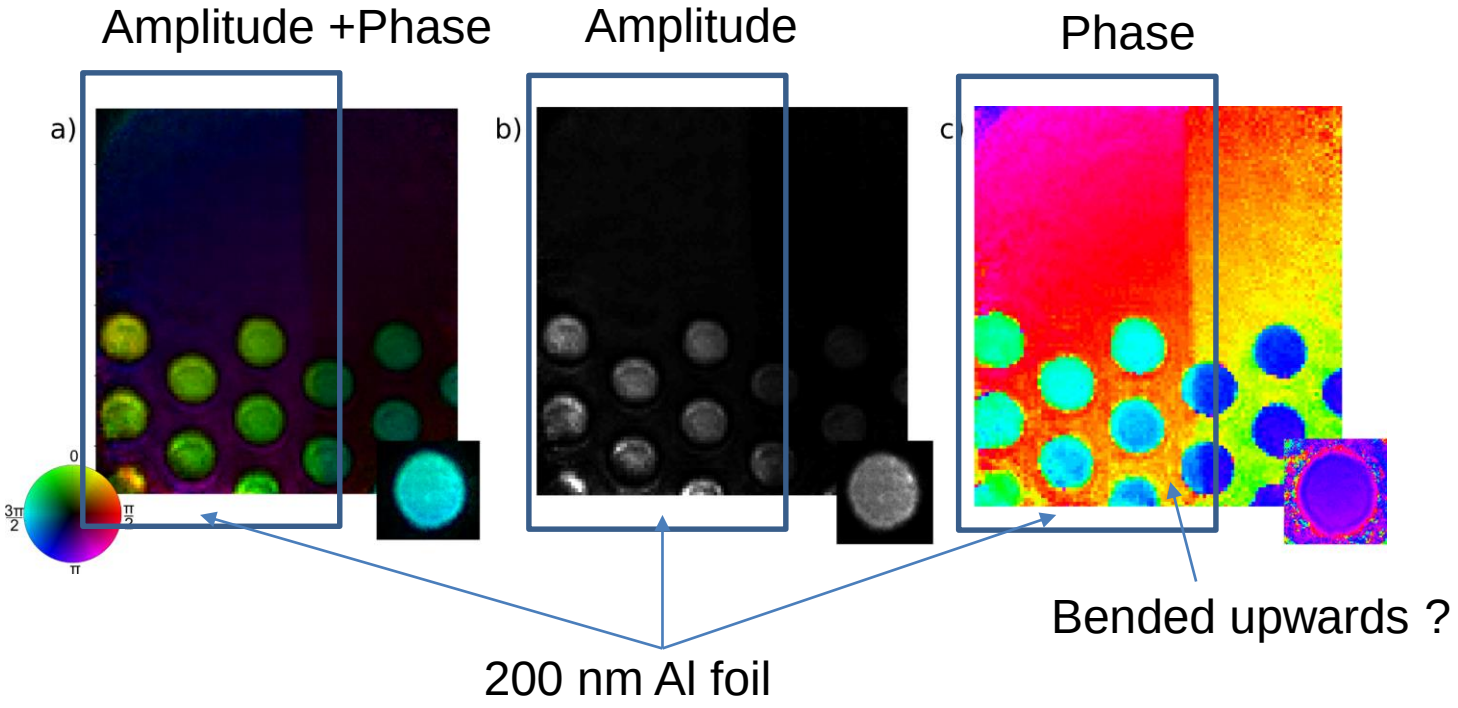

Reflective setup

- Corrections of diffraction pattern due to inclined incident light required
- Alignment of scanning position and programmed defect array challenging
- Camera, sample & deflection mirror dimensions are strong limitations for set-up

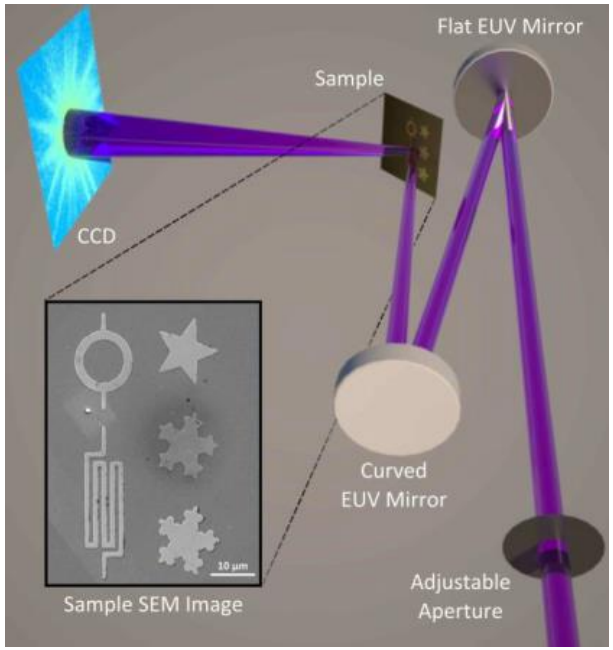

Zhang, B., et al.. SPIE (2014): height resolution of ~ 1 nm and spatial resolution of 1.3·λ achieved

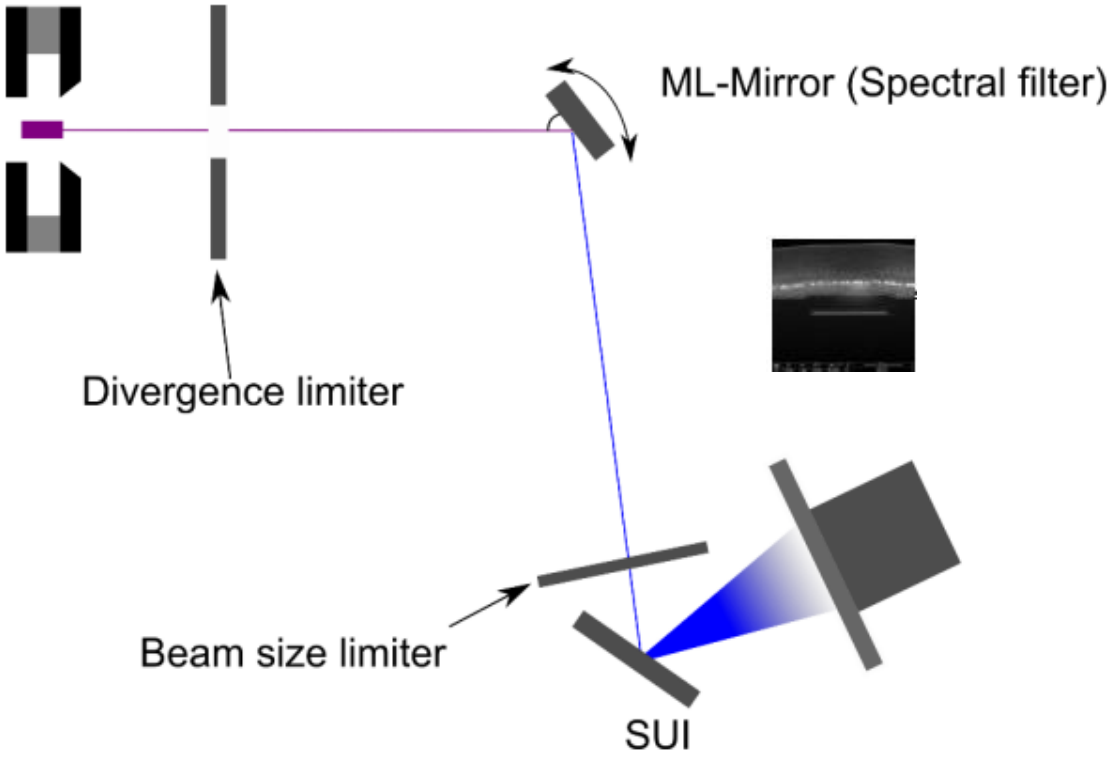

Conclusions and outlook

+ Phase and amplitude information
+ Beam metrology
+ No need of traditional optics
- Requirement of coherent and stable illumination

- Proof-of-principle CDI and ptychographic imaging experiments have been performed with compact, laboratory scale, gas discharge plasma based EUV sources. Successful imaging has been demonstrated despite only partially coherent EUV illumination.
- Linear correction method is developed to account for imperfect coherence of the illumination probe and to remove visible light background in the diffraction patterns.
- Beam-divergence limiting apertures are used in experiments along with numerical deconvolution methods to compensate imperfect coherence. Coherent photon flux at the detector is on the order of 10^4 – 10^5 photons/s.
- The EUV sources with narrow resonant line emission ($\lambda/\Delta\lambda > 10^3$-$10^5$) in combination with high spectral selectivity of gratings and/or Bragg-mirrors for wavelength discrimination enable spectrally resolved CDI experiments with elemental sensitivity.

Thank you very much for your attention!

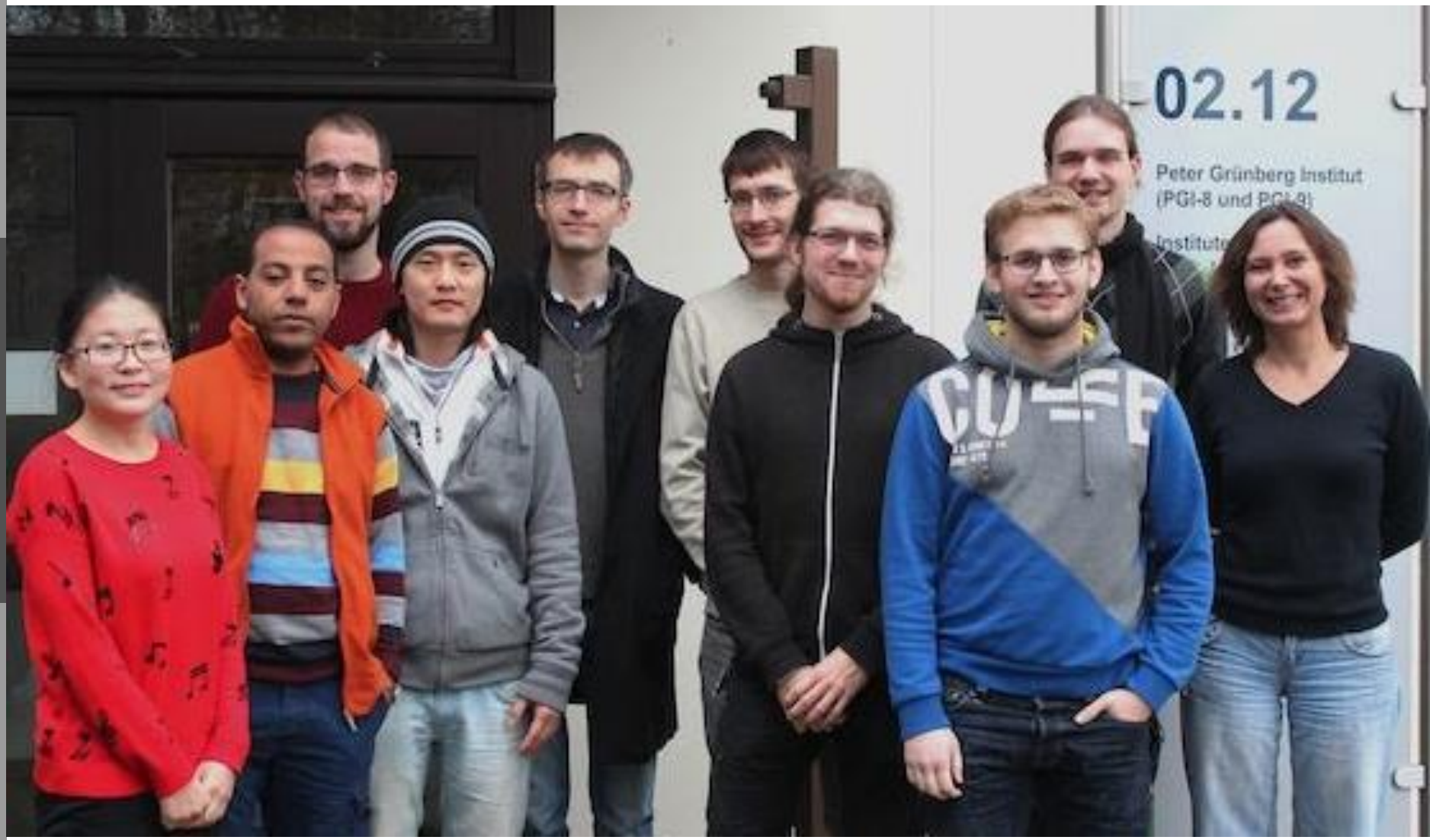

Coherent Diffraction Imaging

- Imaging of (non-crystalline) objects without lenses/mirrors
- Recording of far-field diffraction patterns
  - ⇒ Resolution limited by wavelength / NA of detector
  - ⇒ Recovery of phase and amplitude of the transmitted wave / real space
- Detector records the Fourier space intensity distribution
- Oversampling required to retrieve the phase
- Simple and low-cost setup
  - ⇒ Optics is replaced by computational algorithms

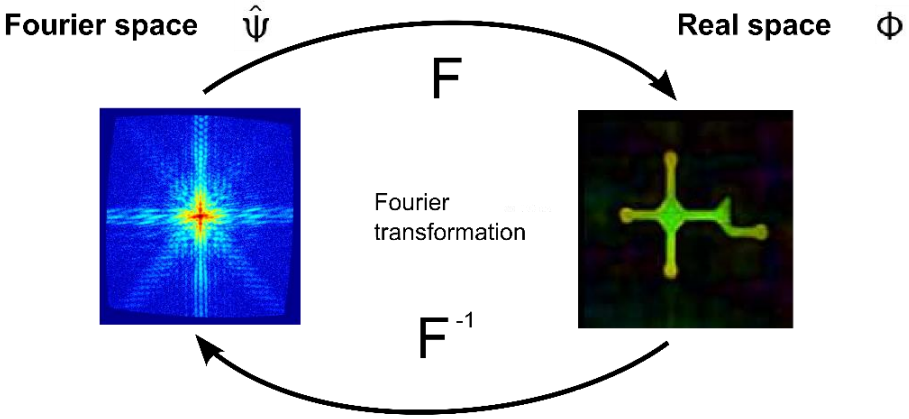

First demonstration of CDI:

J. Miao et al., "Extending the methodology of X-ray crystallography to allow imaging of micrometre-sized non-crystalline specimens", *Nature* **400**, 342 (1999)

Comprehensive Overview:

P. Thibault, "Algorithmic methods in diffraction microscopy", Dissertation, Cornell University, 2007

J. Miao et al., "Beyond crystallography: Diffractive imaging using coherent x-ray light sources", Science **348** (6234), 530 (2015)

Spatial Coherence

- 4 π emitter => divergent source with Lorentzian pinch plasma (750 µm FWHM)
- 500 µm aperture limits divergence < 1.5 mrad => ~ 80 nJ per pulse (@ 1kHz)
- (single exposure) coherence determination by double slit array

$$I(x,y) = I_0 \left[1 + g_{12} \cos\left(\frac{2\pi d}{\lambda z} x + \beta\right)\right] sinc^2\left(\frac{\pi D}{\lambda z} x\right)$$

D: slit width, d: slit separation, z: distance slits-detector, x: position on the screen from center spot, γ_{12}: mutual coherence function with $\gamma_{12} = g_{12} e^{i\beta}$, I_0: 2x intensity on single slit

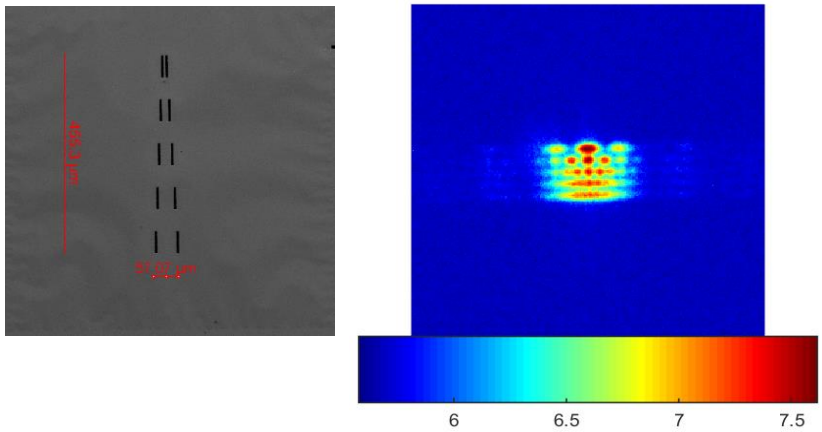

D. Paterson, *Opt. Commun.*, *195* (1-4), 79–84, 2001

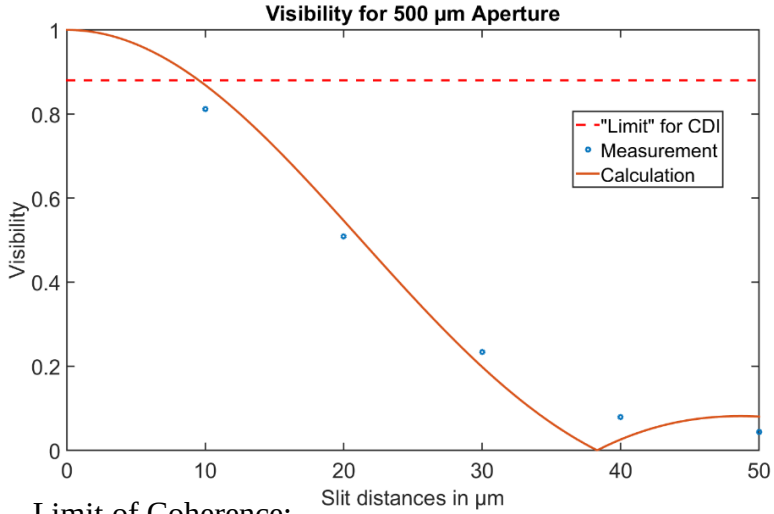

Limit of Coherence:
M. Born and E. Wolf, *Principles of Optics*, Cambridge, 1999
Calculation with Van-Zittert-Cernike theorem

CDI Reconstruction

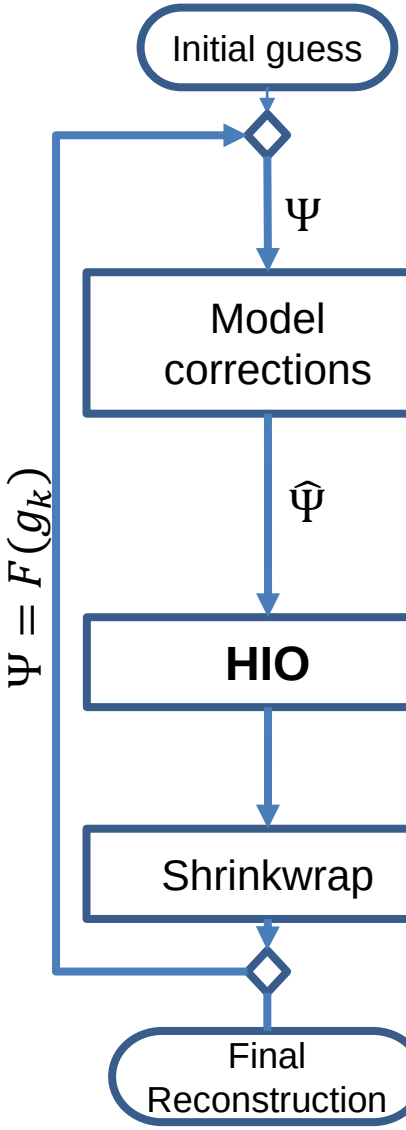

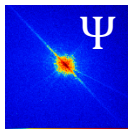

Triple Intersection estimate

Fienup, J. R. (1988). Fourier intensity data (Vol. 828, pp. 13–19)

Marchesini, S. et al., *PRB*, 68, 2003

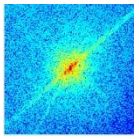

$$\left|\breve{\Psi}\right|^2 = (|\Psi|^2 * PSF)(k_x, k_y) + b$$

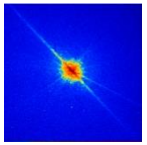

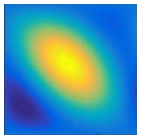

$$\hat{\Psi} = \sqrt{\frac{I}{\left|\breve{\Psi}\right|^2}}\,\Psi$$

- Fitting of difference between measurement and reconstruction by scaled reconstruction
- Improved high frequency noise

$$g_k = F^{-1}(\hat{\Psi})$$

- Feedback constant β is slowly increased to 1

$$g_{k+1} = \begin{cases} g_k - \beta g'_k, & x \notin mask \\ (1-\beta)g_k + \beta^2 g'_k, & x \in mask \end{cases}$$

Fienup, J.R, *Opt. Lett.*, 3, 27-29, 1978

Clark, J. N. et al., *APL.*, 99, 2011

- Adapted mask size during reconstruction
- Error metric

Marchesini, S. et al., *PRB*, 68, 2003

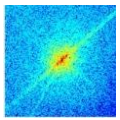

Background diffraction subtraction

- Longer wavelengths generate overlapping diffraction patterns
- Filtering removes the UV/Visible light but with loss of overall intensity
- (Realistic) assumption:
  - Low intensity
  - Coherent

⇒ Upscaling of the reconstructed diffraction pattern

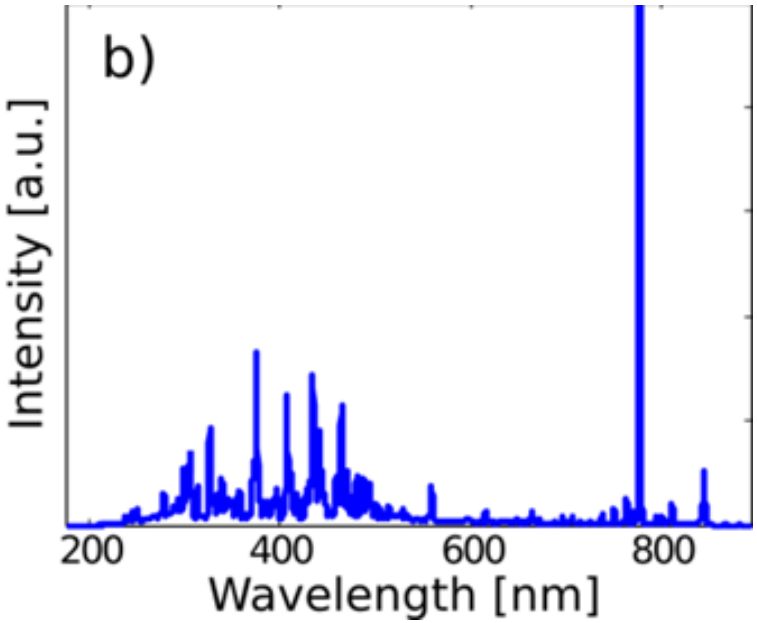

$$b_{n+1,j} = \alpha_n \left| F^{-1}\left[F\left(W_n\left(\widehat{\psi_j} - \psi_j - b_{n,j}\right) + b_{n,j}\right) * \frac{P_{vis}}{\max P_{vis}} \right] \right| + (1-\alpha) b_{n,j}$$

α, W are constant just for optimization

Background diffraction subtraction

$$b_j = I_{recorded} - |\Psi_{reconstructed}(k)|^2$$

- Iterative optimization of background
- Updating background multiple times during CDI reconstruction

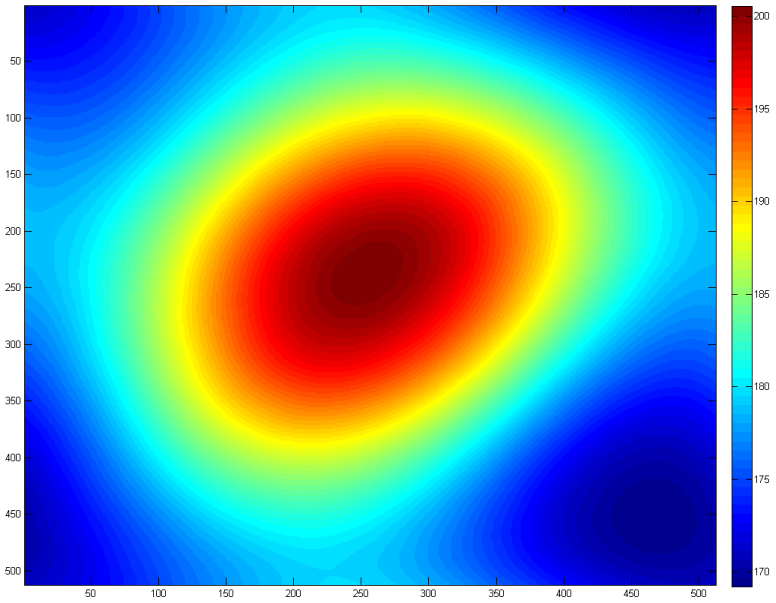

Measurements

Grid Settings:

7 x 7 grid

2.3 µm step size
=> 70 % overlap

=> ~ 25 x 25 µm FOV

Camera/ Exposure Settings:

- 60 °C

50 kHz read-out
(256 x 256 pixels)

t_exp= 60 s

f_rep ~450 Hz

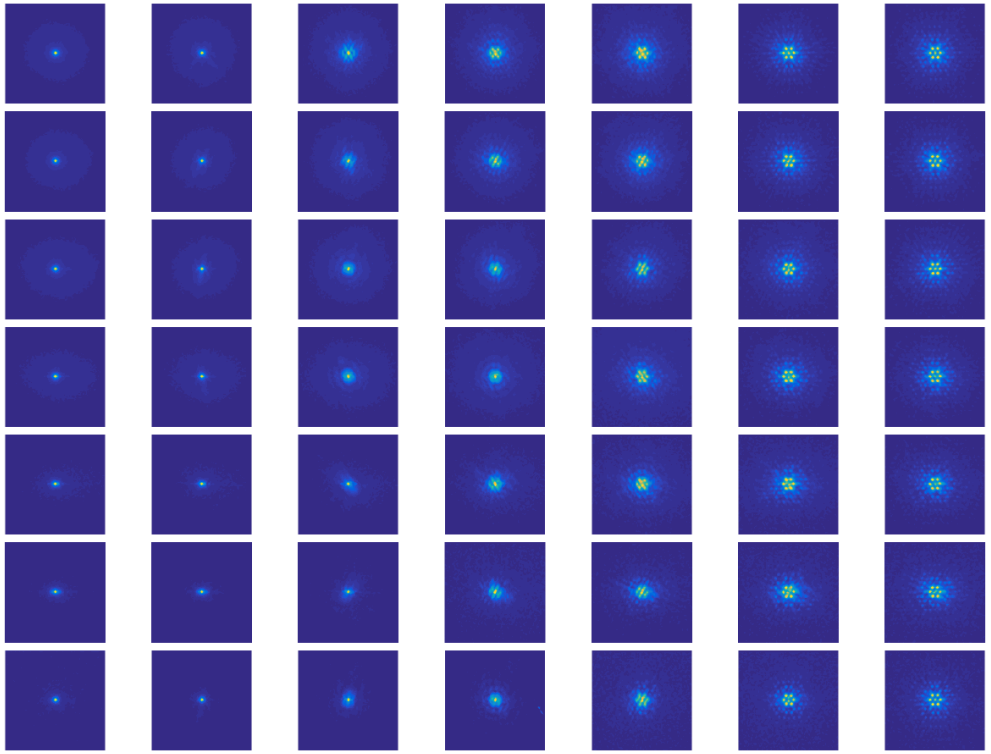

Phase diffraction gratings

- Moderate efficiency
- Adjustable working wavelength and spectral resolution
- Selection of emission lines enables material contrast